

Diffraction of water waves for vertical cylinders using boundary elements

M. C. Au and C. A. Brebbia

Department of Civil Engineering, University of Southampton, Southampton, UK
(Received November 1982)

This paper presents the application of the boundary element method for computing wave forces on offshore structures of constant section throughout the depth of water. The paper compares results obtained using constant, linear and quadratic elements and draws some original conclusions regarding their numerical accuracy and convergence. Examples studied include the vertical circular cylinder, the square caisson and the elliptical cylinder for which the boundary element solutions are compared against analytical or experimental results. The paper also shows how symmetry conditions can be introduced into the problem to reduce the computer storage and time required to solve the problems.

Key words: mathematical model, BEM, offshore structures, wave forces

Introduction

The close form solution for the horizontal force on a vertical circular cylinder subject to linear water waves was given by MacCamy and Fuchs.¹ Two decades later vertical elliptical cylinder solutions were attained by Goda and Yoshimura.² These two special cases of wave diffraction for structures of constant horizontal section were generalized for arbitrary shape cylinders by Ijima, Chung and Yumura,³ who studied the case of permeable and impermeable breakwaters. The use of isolated structures using integral equation techniques were also given by Isaacson⁴ and later by Harns.⁵ A problem mathematically similar to wave diffraction is the study of harbour oscillations, such as described by Hwang and Tuck⁶ for harbours of arbitrary shape. Recently Rahman⁷ has extended this formulation to calculate the response of harbours with regions of different depths.

All the above problems are governed by the two-dimensional Helmholtz equation as the governing equation. The fundamental solution for this equation is well known and given in terms of a Hankel function. The newly developed boundary element technique⁸⁻¹⁰ has been successfully applied to solve many engineering problems such as potential, elastostatics, time dependent cases and even nonlinear material problems. The technique is extended here to study the wave diffraction behaviour of offshore structures of generalized cylindrical shape. The paper compares results obtained using constant, linear and quadratic elements and critically discusses their numerical accuracy and convergence. Specific examples considered include the vertical circular cylinder, the square caisson

and the elliptical cylinder for which the boundary element solutions are compared against analytical or experimental results. The paper also shows how to introduce symmetry conditions into the problem to reduce the computer storage and time required to run the problems.

Boundary value formulation

The wave diffraction of an incident wave represented by its potential Φ^I on a general three-dimensional body can be represented by the diffracted potential Φ^s governing equation, i.e.:

$$\nabla^2 \Phi^s = \frac{\partial^2 \Phi^s}{\partial x^2} + \frac{\partial^2 \Phi^s}{\partial y^2} + \frac{\partial^2 \Phi^s}{\partial z^2} = 0 \quad \text{in } \Omega(x, y, z) \quad (1)$$

with the boundary conditions, $(\Phi = \Phi^s)$ say:

$$\begin{aligned} \frac{\partial \Phi}{\partial n} + \frac{\partial \Phi^I}{\partial n} &= 0 && \text{on surface of body, } \Gamma_c \\ \frac{\partial \Phi}{\partial n} &= 0 && \text{at bottom of sea, } \Gamma_b \\ \frac{\partial \Phi}{\partial n} - i\kappa \Phi &= 0 && \text{at infinity, } \Gamma_\infty \\ \frac{\partial \Phi}{\partial n} - \frac{\omega^2}{g} \Phi &= 0 && \text{on free surface, } \Gamma_s \end{aligned} \quad (2)$$

where Φ^I is the total potential $\Phi^I = \Phi^I + \Phi$. Note that the incident wave also satisfies the Laplace equation (1), i.e. $\nabla^2 \Phi^I = 0$.

The incident wave potential for a linear wave is given by:

$$\Phi^I = -\frac{iga_0}{\omega \cosh \kappa h} \cosh \kappa Z \cdot \exp\{i(K_1 x + K_2 y - \omega t)\} \tag{3}$$

where a_0 is the wave amplitude, h is the water depth, g the gravity constant, ω the wave frequency, κ the wave number and α the angle of the incident wave, K_1 and K_2 are:

$$K_1 = \kappa \cos \alpha \quad K_2 = \kappa \sin \alpha$$

The above formulation can be simplified when the horizontal surface of the body is constant with depth. One can now assume that the total potential can be written as:

$$\Phi = \phi \cosh \kappa Z \tag{4}$$

Substituting this into (1) we have:

$$\frac{\partial^2 \phi}{\partial x^2} + \frac{\partial^2 \phi}{\partial y^2} + \kappa^2 \phi = 0 \quad \text{in } \Omega(x, y) \tag{5}$$

with the boundary condition:

$$\frac{\partial \phi}{\partial n} + \frac{\partial \phi^I}{\partial n} = 0 \quad \text{on } \Gamma_c \tag{6}$$

$$\frac{\partial \phi}{\partial n} - i\kappa \phi = 0 \quad \text{on } \Gamma_\infty \text{ (at infinity)}$$

The other boundary conditions are satisfied by Φ as:

$$\kappa \tanh \kappa h = \frac{\omega^2}{g} \tag{7}$$

The incident wave is now:

$$\phi^I = -\frac{iga_0}{\omega \cosh \kappa h} \exp\{i(K_1 x + K_2 y)\} \tag{8}$$

The above problem can be extended to the water of variable depths by the formulation given by Berkhoff.¹¹

Boundary element integrals

One can now apply the weighted residual formulation⁸ to the water system of equations represented by (5) and (6). If ϕ^* is defined as the weighting function, one can write:

$$\int_{\Omega} (\nabla^2 \phi + \kappa^2 \phi) \phi^* \, d\Omega = \int_{\Gamma_c} \left(\frac{\partial \phi}{\partial n} + \bar{q} \right) \phi^* \, d\Gamma + \int_{\Gamma_\infty} \left(\frac{\partial \phi}{\partial n} - i\kappa \phi \right) \phi^* \, d\Gamma \tag{9}$$

where $\bar{q} = \partial \phi^I / \partial n$.

Integrating the first term in the left-hand side of equation (9) by parts twice, one can obtain:

$$\int_{\Omega} (\nabla^2 \phi^* + \kappa^2 \phi^*) \phi \, d\Omega = \int_{\Gamma_c} \bar{q} \phi^* \, d\Gamma + \int_{\Gamma_c + \Gamma_\infty} \phi \frac{\partial \phi^*}{\partial n} \, d\Gamma - \int_{\Gamma_\infty} i\kappa \phi^* \phi \, d\Gamma \tag{10}$$

Notice that ϕ^* can be taken as the fundamental solution of the following equation:

$$\nabla^2 \phi^* + \kappa^2 \phi^* = -\Delta_i \tag{11}$$

where Δ_i is a delta function at (ξ, η) . The form of ϕ^* is:

$$\phi^* = \frac{i}{4} H_0^1(\kappa |r|) \tag{12}$$

with $|r| = [(x - \xi)^2 + (y - \eta)^2]^{1/2}$ and $H_0^1(\cdot)$ is the Hankel function of the first kind and of zero order.

For a point 'i' inside the Ω domain equation (10) now becomes:

$$\phi_i + \int_{\Gamma_c} \left(\frac{\partial \phi^*}{\partial n} \phi + \phi^* \bar{q} \right) \, d\Gamma + \int_{\Gamma_\infty} \left(\frac{\partial \phi^*}{\partial n} - i\kappa \phi^* \right) \phi \, d\Gamma = 0 \tag{13}$$

If we consider the last term in equation (13), we can write the fundamental solution when $r \rightarrow \infty$ as:

$$\phi^* \approx \frac{i}{4\sqrt{\pi\kappa r}} \exp\left\{i\left(\kappa r - \frac{\pi}{4}\right)\right\} \tag{14}$$

which gives:

$$\frac{\partial \phi^*}{\partial n} = \frac{\partial \phi^*}{\partial r} = -\frac{\kappa}{4\sqrt{\pi\kappa r}} \exp\left\{i\left(\kappa r - \frac{\pi}{4}\right)\right\} \tag{15}$$

Notice that these solutions will identically satisfy the radiation condition, i.e.:

$$\frac{\partial \phi^*}{\partial n} - i\kappa \phi^* = 0 \tag{16}$$

As ϕ^* satisfies the boundary conditions on Γ_∞ , the last integral in equation (13) disappears and that integral expression simplifies to:

$$\phi_i + \int_{\Gamma_c} \left(\frac{\partial \phi^*}{\partial n} \phi + \phi^* \bar{q} \right) \, d\Gamma = 0 \tag{17}$$

Let us now consider what happens when the 'i' point is on the boundary Γ_c (Figure 1). The boundary integral in (17) can be written as:

$$\phi_i + \lim_{\epsilon \rightarrow 0} \left\{ \int_{\Gamma_c - \Gamma_\epsilon} \left(\frac{\partial \phi^*}{\partial n} \phi + \phi^* \bar{q} \right) \, d\Gamma + \int_{\Gamma_\epsilon} \left(\frac{\partial \phi^*}{\partial n} \phi + \phi^* \bar{q} \right) \, d\Gamma \right\} = 0 \tag{18}$$

The limit for the first integral in (18) is:

$$\lim_{\epsilon \rightarrow 0} \left\{ \int_{\Gamma_c - \Gamma_\epsilon} \left(\frac{\partial \phi^*}{\partial n} \phi + \phi^* \bar{q} \right) \, d\Gamma \right\} = \int_{\Gamma_c} \left(\frac{\partial \phi^*}{\partial n} \phi + \phi^* \bar{q} \right) \, d\Gamma \tag{19}$$

While the limit for the second integral can be written as:

$$\lim_{\epsilon \rightarrow 0} \left\{ \int_{\Gamma_\epsilon} \frac{\partial \phi^*}{\partial n} \phi \, d\Gamma \right\} = \lim_{\epsilon \rightarrow 0} \left\{ \int_{\Gamma_\epsilon} \frac{\partial \phi^*}{\partial n} \, d\Gamma \right\} \phi_i \tag{20}$$

$$\lim_{\epsilon \rightarrow 0} \left\{ \int_{\Gamma_\epsilon} \phi^* \bar{q} \, d\Gamma \right\} = \lim_{\epsilon \rightarrow 0} \left\{ \int_{\Gamma_\epsilon} \phi^* \, d\Gamma \right\} \bar{q}_i \tag{21}$$

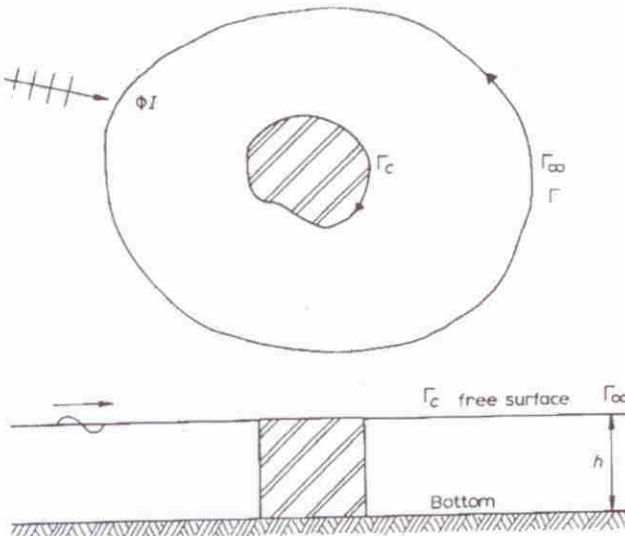


Figure 1 Structure with constant horizontal section

In order to calculate these limits we can use the approximate expansion of the Hankel function up to the order $(\kappa|r|)^2$, which is given by:

$$\phi^* = -\frac{1}{2\pi} \left[\gamma + \ln\left(\frac{\kappa|r|}{2}\right) \right] + \frac{i}{4} \quad (22)$$

where γ is the Euler's constant ($\gamma = 0.577216\dots$) and hence:

$$\frac{\partial \phi^*}{\partial r} = -\frac{1}{2\pi|r|} \quad (23)$$

Substituting (23) into (20) we find:

$$\lim_{\epsilon \rightarrow 0} \left\{ \int_{\Gamma_\epsilon} \frac{\partial \phi^*}{\partial n} d\Gamma \right\} = \lim_{\epsilon \rightarrow 0} \left\{ \int_0^\alpha \left(-\frac{1}{2\pi\epsilon} \epsilon d\theta \right) \right\} = -\frac{\alpha}{2\pi} \quad (24)$$

where α is the angle at the point 'i' under consideration (Figure 2).

One can now use (22) and substitute it into (21) which gives:

$$\lim_{\epsilon \rightarrow 0} \left\{ \int_{\Gamma_\epsilon} \phi^* d\Gamma \right\} = \lim_{\epsilon \rightarrow 0} \left\{ \int_0^\alpha \left(-\frac{1}{2\pi} \left(\gamma + \ln\frac{\kappa\epsilon}{2} \right) + \frac{i}{4} \right) \epsilon d\theta \right\} = 0 \quad (25)$$

Hence, the boundary integral formulation for a point on the boundary can be written:

$$c_i \phi_i + \int_{\Gamma_c} \left(\frac{\partial \phi^*}{\partial n} \phi + \phi^* \bar{q} \right) d\Gamma = 0 \quad (26)$$

where $c_i = 1 - \alpha/2\pi$ and $\Gamma = \Gamma_c$ (boundary on the body surface).

The boundary Γ is now discretized into M boundary elements over which the variables can be interpolated as follows, for element 'j':

$$\begin{aligned} \phi_j &= [N] \{ \phi_j^n \} \\ \bar{q}_j &= [N] \{ \bar{q}_j^n \} \end{aligned} \quad (27)$$

The boundary integral equation (26) now becomes:

$$\begin{aligned} c_i \phi_i + \sum_{j=1}^M \int_{\Gamma_j} \frac{\partial \phi^*}{\partial n} [N] d\Gamma \{ \phi_j^n \} \\ = - \sum_{j=1}^M \int_{\Gamma_j} \phi^* [N] d\Gamma \{ \bar{q}_j^n \} \end{aligned} \quad (28)$$

Applying this equation at all 'i' boundary points, the following matrix form is produced:

$$[H] \{ \Phi \} = [G] \{ \bar{Q} \} \quad (29)$$

with:

$$[h_{ij}] = C_i \delta_{ij} + \int_{\Gamma_j} \frac{\partial \phi^*}{\partial n} [N] d\Gamma \quad (30)$$

and

$$[g_{ij}] = \int_{\Gamma_j} \phi^* [N] d\Gamma$$

Note that the potential defined here has real and complex parts, that is:

$$\begin{aligned} \{ \Phi \} &= \{ U \} + i \{ V \} \\ \{ \bar{Q} \} &= \{ R \} + i \{ S \} \end{aligned} \quad (31)$$

Equation (29) can now be written in matrix form as:

$$\begin{bmatrix} H_1 & -H_2 \\ H_2 & H_1 \end{bmatrix} \begin{bmatrix} U \\ V \end{bmatrix} = \begin{bmatrix} G_1 & -G_2 \\ G_2 & G_1 \end{bmatrix} \begin{bmatrix} R \\ S \end{bmatrix} \quad (32)$$

where $[H] = [H_1] + i[H_2]$ and $[G] = [G_1] + i[G_2]$.

This is the complex system of equations which has to be solved during the analysis.

After the solution of (32), the pressure on the structure can be obtained by the linearized Bernoulli's equation as:

$$P = -\rho \frac{\partial \Phi}{\partial t} \quad (33)$$

and by integrating the pressure in the vertical z direction, the wave forces can be written as:

$$\bar{F} = i\rho\omega \frac{\sinh kh}{k} \int_{\tau} \begin{bmatrix} n_x \\ n_y \end{bmatrix} \phi d\tau \quad (34)$$

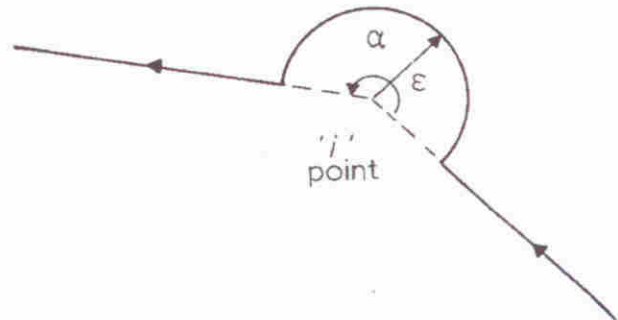


Figure 2 i point on boundary

Integration over elements

We will now study how the integrals over the elements can be carried out taking into consideration the three different types of elements, i.e. constant, linear and quadratic. For the constant element integrals such as:

$$\int_{\Gamma_j} \frac{\partial \phi^*}{\partial n} d\Gamma \quad \text{and} \quad \int_{\Gamma_j} \phi^* d\Gamma \quad (35)$$

can be integrated numerically when $i \neq j$, usually applying a standard four points Gauss integration rule. When $i = j$ the first of the above integrals is identically zero due to the orthogonality between n and Γ ($\partial r / \partial n = 0$) and the second integral can be integrated analytically, i.e.:

$$\int_{\Gamma_i} \phi^* d\Gamma = \Gamma_i \left\{ \frac{1}{2\pi} \left[1 - \gamma - \ln \left(\frac{\kappa \Gamma_i}{4} \right) + \frac{i}{4} \right] \right\} \quad (36)$$

At the same time as for a constant element, the 'i' point is taken to be on the mid-point of the element, α is equal to π and c_i becomes:

$$c_i = \frac{1}{2}$$

The interpolation functions for linear elements are:

$$[N] = \left[\frac{1-\xi}{2}, \frac{1+\xi}{2} \right] \quad (-1 < \xi < 1) \quad (37)$$

For the case $i \neq j$ the integration can be carried out using numerical quadrature formulae as discussed for the constant element. For $i = j$ the first of integrals (35) also disappear and the second after analytical integration gives the following terms:

$$[g_{ij}] = \left[\frac{\Gamma_i}{4\pi} \left(1.5 - \gamma - \ln \frac{\kappa \Gamma_i}{2} \right) + \frac{\Gamma_i}{8} i \right. \\ \left. \times \frac{\Gamma_i}{4\pi} \left(0.5 - \gamma - \ln \frac{\kappa \Gamma_i}{2} \right) + \frac{\Gamma_i}{8} i \right] \quad (38)$$

with $[h_{ij}] = [0] + [c_{ij}]$.

The constant c_i contributing the h_{ij} terms can be calculated from the intersection angle α form by the adjoint element at node i (Figure 3).

$$[h_{ij}] = \begin{bmatrix} 0 & 0 \\ 0 & 0 \end{bmatrix} + \begin{bmatrix} 1 - \frac{\alpha}{2\pi} & 0 \\ 0 & 1 - \frac{\alpha}{2\pi} \end{bmatrix} \quad (39)$$

The integrations over quadratic elements are more complex due not only to the higher order functions involved, but also to the possibility of transferring the coordinates into curvilinear ones which follow better the shape of the body. The interpolation function for quadratic elements is:

$$[N] = \left[\frac{1}{2}(\xi-1)\xi, (1+\xi)(1-\xi), \frac{1}{2}(1+\xi)\xi \right] \quad (40)$$

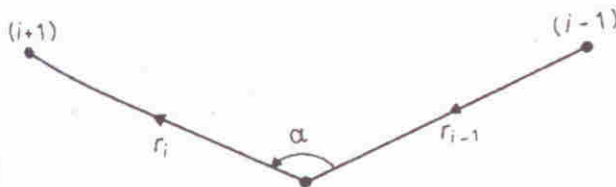
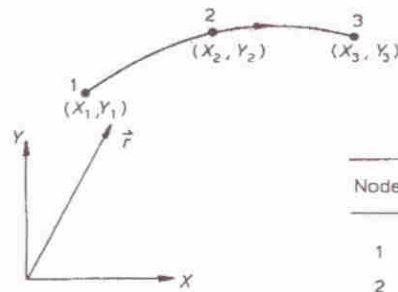


Figure 3 Angle for value c_i



| Node | ξ | N_1 | N_2 | N_3 |
|------|-------|-------|-------|-------|
| 1 | -1 | 1 | 0 | 0 |
| 2 | 0 | 0 | 1 | 0 |
| 3 | 1 | 0 | 0 | 1 |

Figure 4 Quadratic elements

The integrals become:

$$[h_{ij}] = \int_{-1}^1 \frac{\partial \phi^*}{\partial n} [N] |G| d\xi \quad (41)$$

and

$$[g_{ij}] = \int_{-1}^1 \phi^* [N] |G| d\xi \quad (42)$$

where $|G|$ is the Jacobian to transform the system of coordinates to the curvilinear ones shown in Figure 4:

$$|G| = \sqrt{\left(\frac{\partial x}{\partial \xi} \right)^2 + \left(\frac{\partial y}{\partial \xi} \right)^2} \quad (43)$$

Since the geometry of the element needs to be transformed we can define the x and y coordinates also in function of the $[N]$ interpolation shapes, i.e.:

$$x = [N] \{x^n\} \\ y = [N] \{y^n\} \quad (44)$$

and hence:

$$\frac{\partial x}{\partial \xi} = \frac{\partial}{\partial \xi} [N] \{x^n\} \\ \frac{\partial y}{\partial \xi} = \frac{\partial}{\partial \xi} [N] \{y^n\} \quad (45)$$

Now analytical integration is impossible for the case $i = j$ due to the presence of $|G|$ in equations (41) and (42). Notice also that $[h_{ij}]$ is no longer identically zero as now $\partial r / \partial n \neq 0$ in general. A further approximation for ϕ^* can be used, which gives $\partial \phi^* / \partial n$ of order $O((\kappa|r|)^2)$, i.e.:

$$\frac{\partial \phi^*}{\partial n} = - \left\{ \frac{1}{2\pi} \left[\frac{\kappa r}{2} \left(0.5 - \gamma - \ln \frac{\kappa r}{2} \right) + \frac{\kappa r}{8} i \right] \frac{\partial r}{\partial n} \right\} \quad (46)$$

for $i \neq j$ equation (46) substituted into formula (41) gives a non-singular integral which can be integrated numerically using an integration scheme similar to the one previously described. The same applies for integral (42). The term $[g_{ii}]$ ($i = j$) presents a logarithmic singularity and a special integration formula presented in the appendix of reference 8 can be used. The c_i value is calculated as for linear elements.

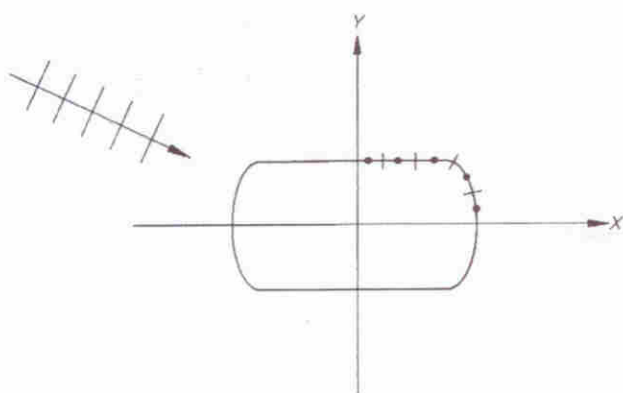


Figure 5 Symmetrical section

Symmetry considerations

When a structure has one or two axes of symmetry, say the x or y axis (Figure 5), one can reduce the computation by using symmetry conditions. Notice that if one starts with the boundary element equation:

$$[H] \{\Phi\} = [G] \{Q\} \quad (47)$$

the symmetry case shown in the figure will allow us to partition the matrix $[H]$ as:

$$[H] = \begin{bmatrix} h_1 & h_2 \\ h_2 & h_1 \end{bmatrix} \quad (48)$$

A transformation matrix can now be defined such that:

$$\{\hat{\Phi}\} = \frac{1}{\beta} [R]^T \{\Phi\} \quad (49)$$

$$\{\hat{Q}\} = \frac{1}{\beta} [R]^T \{Q\}$$

where the transformation matrix $[R]$ is such that:

$$\frac{1}{\beta} [R]^T [R] = [I] \quad (50)$$

The matrix equation (47) can now be written as:

$$[\hat{H}] \{\hat{\Phi}\} = [\hat{G}] \{\hat{Q}\} \quad (51)$$

with

$$[\hat{H}] = \frac{1}{\beta} [R]^T [H] [R] \quad (52)$$

and

$$[\hat{G}] = \frac{1}{\beta} [R]^T [G] [R]$$

Due to the properties of $[R]$, $[H]$ and $[G]$ the resulting $[\hat{H}]$ and $[\hat{G}]$ matrices will have a submatrix on the diagonal (Figure 6). This allows for an economic bounded type storage to be used for $[\hat{H}]$ and $[\hat{G}]$ submatrices.

Each of the diagonal submatrices can be solved independently. Hence the bounded form of $[\hat{H}]$ and $[\hat{G}]$ can be written as $[H^*]$ and $[G^*]$ (Figure 6) such that:

$$\begin{aligned} [H^*] &= [R]^T [H_1] \\ [G^*] &= [R]^T [G_1] \end{aligned} \quad (53)$$

where $[H_1]$ and $[G_1]$ are the first column submatrices of $[H]$ and $[G]$ matrices respectively and the resulting equa-

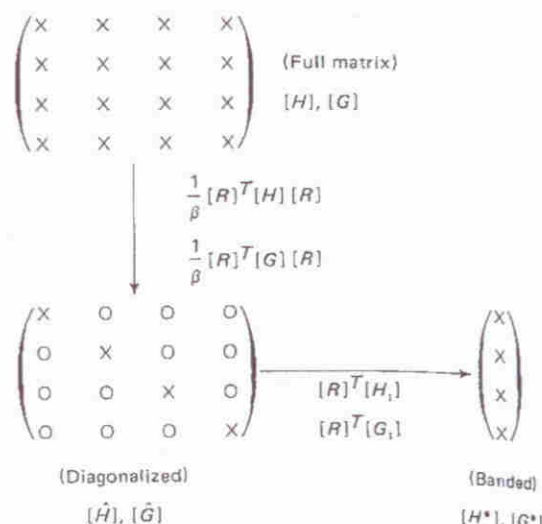


Figure 6 Transformation from full matrix to banded matrix

Table 1 Cases of symmetry

| M_x | 0 | 1 | 2 |
|-------|---|---|--|
| M_y | No symmetry | Symmetry with x -axis, $\alpha = 0^\circ$ | Symmetry with x -axis, $\alpha \neq 0^\circ$ |
| 1 | Symmetry with y -axis, $\alpha = 90^\circ$ | | Symmetry with x - and y -axes, $\alpha = 90^\circ$ |
| 2 | Symmetry with y -axis, $\alpha \neq 90^\circ$ | Symmetry with x - and y -axes, $\alpha = 0^\circ$ | Symmetry with x - and y -axes, $\alpha \neq 0^\circ, 90^\circ$ |

tions can be symbolized by:

$$[H^*] \{\hat{\Phi}\} = [G^*] \{\hat{Q}\} \quad (54)$$

We can now consider the types of symmetry that can be used for the two-dimensional problem represented in Figure 5. They are represented in Table 1.

The M_x and M_y represents the symmetry number. M_x and M_y are the indexes assigned to the symmetry conditions about the x -axis and y -axis respectively and their definitions are given in Table 1.

The matrix $[R]^T$ computing to the symmetry cases of Table 1 are given in Table 2.

It is necessary to apply the image method⁹ to calculate the $[H_1]$ and $[G_1]$ matrices and hence transform the point under consideration according to different symmetry conditions. The relative image position which is parallel to $[R]^T$ gives one:

$$\begin{aligned} 1st & (x, y) \\ 2nd & (-x, y) \\ 3rd & (x, -y) \\ 4th & (-x, -y) \end{aligned} \quad (55)$$

These conditions are used for $[H^*]$ and $[G^*]$. The solution is obtained by solving (53) and the actual values of $\{\Phi\}$ and $\{Q\}$ can then be calculated, i.e.:

$$\begin{aligned} \{\Phi\} &= [R] \{\hat{\Phi}\} \\ \{Q\} &= [R] \{\hat{Q}\} \end{aligned} \quad (56)$$

Table 2 Matrix $[R]^T$ and value β

| | M_x | 0 | 1 | 2 |
|-------|-------|--|---|---|
| M_y | | | | |
| 0 | | $[1], \beta=1$ | $[1 \ 1], \beta=2$ | $\begin{bmatrix} 1 & -1 \\ 1 & 1 \end{bmatrix}, \beta=2$ |
| 1 | | $[1 \ -1], \beta=2$ | | $\begin{bmatrix} 1 & 1 & 1 & 1 \\ -1 & -1 & 1 & 1 \end{bmatrix}, \beta=4$ |
| 2 | | $\begin{bmatrix} 1 & -1 \\ 1 & 1 \end{bmatrix}, \beta=2$ | $\begin{bmatrix} 1 & 1 & 1 & 1 \\ -1 & 1 & -1 & 1 \end{bmatrix}, \beta=4$ | $\begin{bmatrix} 1 & 1 & 1 & 1 \\ -1 & 1 & -1 & 1 \\ -1 & -1 & 1 & 1 \\ 1 & -1 & -1 & 1 \end{bmatrix}, \beta=4$ |

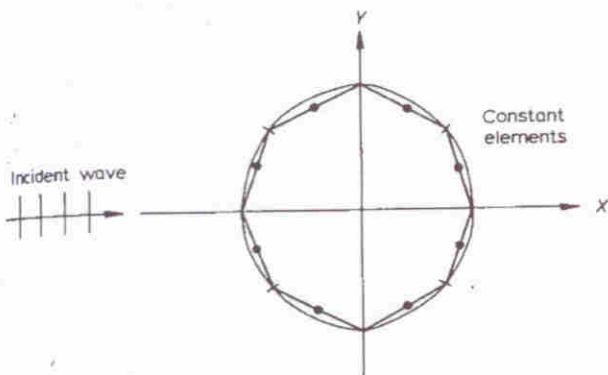


Figure 7 Vertical circular cylinder. $a = 10$; $h/a = 5$; $N = 6, 12, 14$

Applications

The technique will now be applied to study the wave diffraction behaviour of offshore structures of generalized cylindrical shape. Results are compared using constant, linear and quadratic elements and their numerical accuracy and convergence is critically discussed. The specific examples included are: a vertical circular cylinder; a square caisson; and an elliptical cylinder (with and without symmetry).

Vertical circular cylinder

The horizontal wave force on the vertical circular cylinder shown in Figure 7 were first obtained by using different boundary element discretizations. This case has been studied by Isaacson⁴ using sources distributed over the boundary (i.e. indirect boundary element method) and by MacCamy and Fuchs¹ who found the exact solution for the horizontal forces, i.e.:

$$F_x = H'_1(\kappa R) \rho g a_0 R h \frac{\tanh \kappa h}{\kappa h} \tag{57}$$

The magnitude and the phase were also presented and compared against boundary element results. The first boundary element solution consisted in dividing the cylinder into a mesh of 6, 12 and 24 constant elements (Figure 8). The magnitude of the forces F_x given by the 6 and 12 element mesh were within 7 and 2% respectively of the exact value. Excellent agreement in the magnitude of the force and its phase were obtained by using 24 elements

(Figures 8 and 9). Higher order (linear and quadratic) elements were then used and convergence was studied using constant, linear and quadratic elements. As shown in Figure 10, quadratic elements gave the more accurate results. It is interesting to note that the convergence of the constant elements is superior to that of linear ones. This surprising result was thought to be due to the difficulty of representing properly the normal at the corner for linear elements. The convergence for the phase of F_x is also given (Figure 11).

Square caisson

The example of a square caisson as shown in Figure 12 has been studied by Mogridge and Jamieson.¹² They performed an experiment on a 12 in x 12 in square box in a

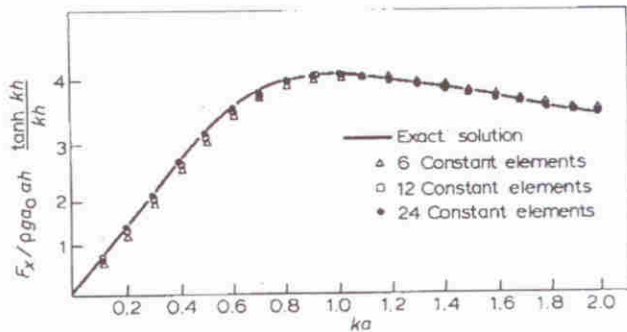


Figure 8 Horizontal force on vertical cylinder ($a = 10$)

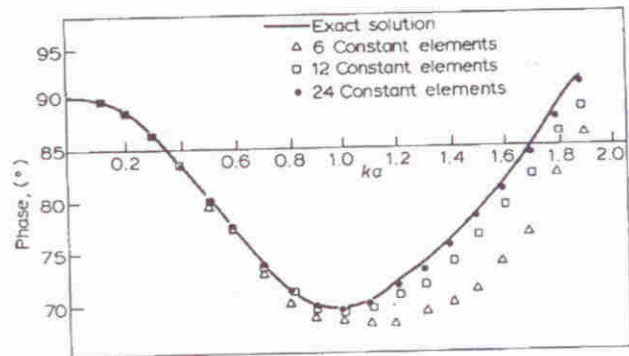


Figure 9 Phase of horizontal force on vertical cylinder ($a = 10$)

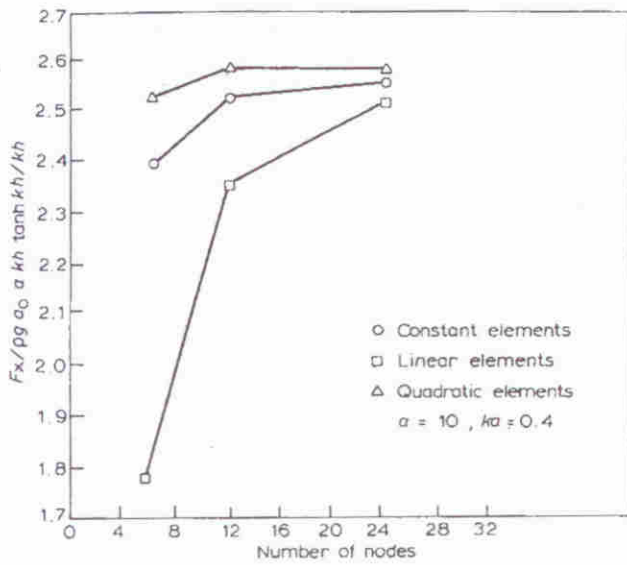


Figure 10 Convergence of horizontal force on a vertical cylinder

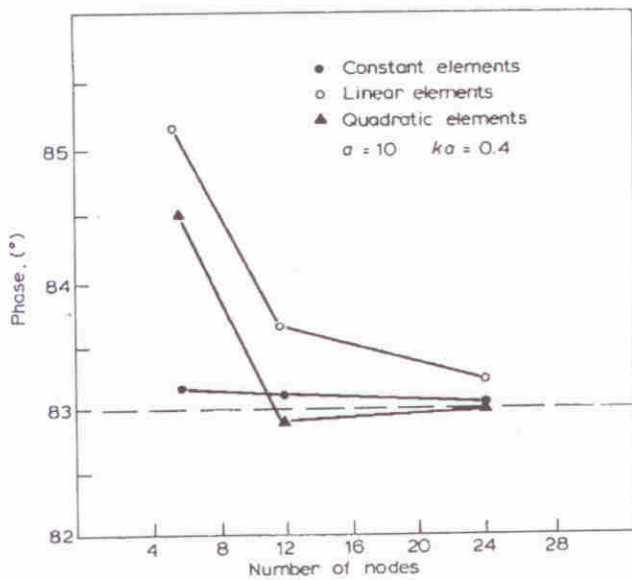


Figure 11 Convergence of phase of horizontal force on a vertical cylinder

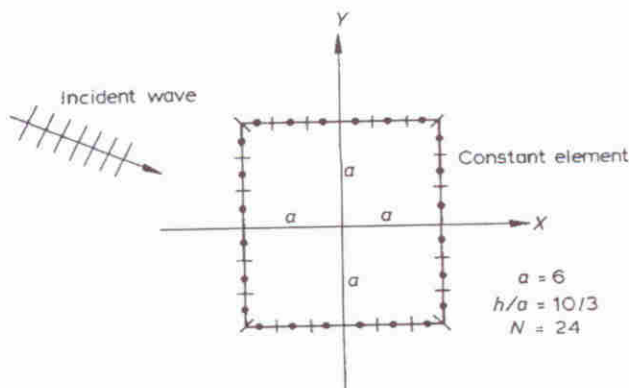


Figure 12 Element discretization of a square caisson (2a x 2a)

wave flume 12 ft wide, 4.5 ft deep and 162 ft long. Experimental results for horizontal wave forces with $\alpha = 0^\circ$ and 45° were measured and using the theory of equivalent circular radius, i.e.:

$$R_e = 2A/\sqrt{\pi} \tag{58}$$

(where $2A$ is the side of the square) formula (52) valid for a cylinder can be applied as an approximation.

The boundary element method was applied using 24 constant boundary elements and the results for magnitude and phase of the horizontal forces are compared in Figures 13 and 14 against those presented by Mogridge and Jamieson. Good agreement was found for the case of $\alpha = 0$ (Figure 13) but for $\alpha = 45^\circ$ (Figure 14) the phase as given by boundary elements differs from the results presented in reference 11.

It can be concluded that the magnitude of the horizontal force on a square section is only slightly altered by the angle of attack of the incident wave and agree reasonably well with the equivalent cylinder results. The phase, however, can only be approximately reproduced by the equivalent cylinder approach and the boundary element method is a better analytical technique. (Note that for the equivalent cylinder approach the angle of attack does not change either the magnitude or the phase of the horizontal force.) This is an interesting conclusion as most caisson

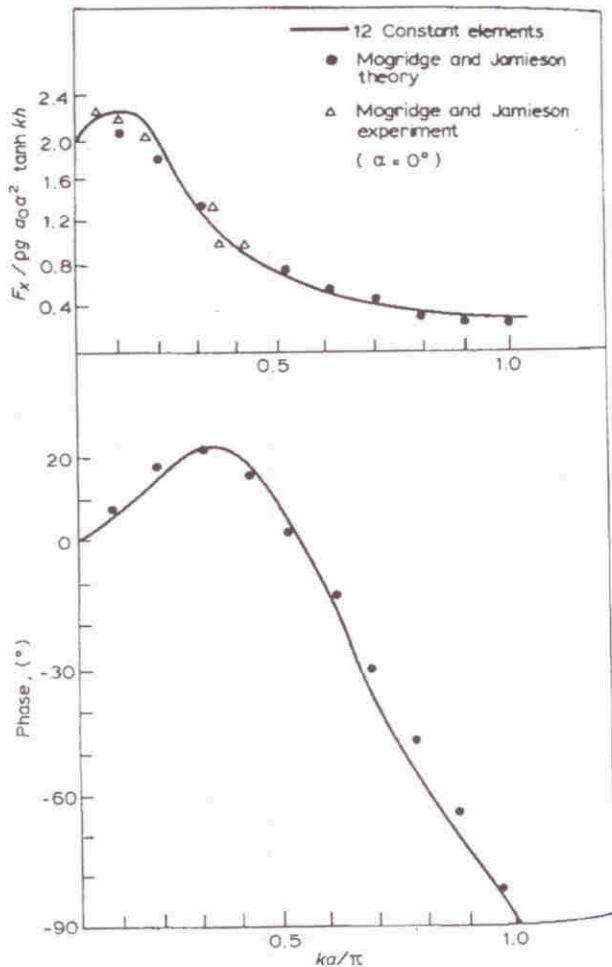


Figure 13 Magnitude and phase of horizontal force on a square caisson

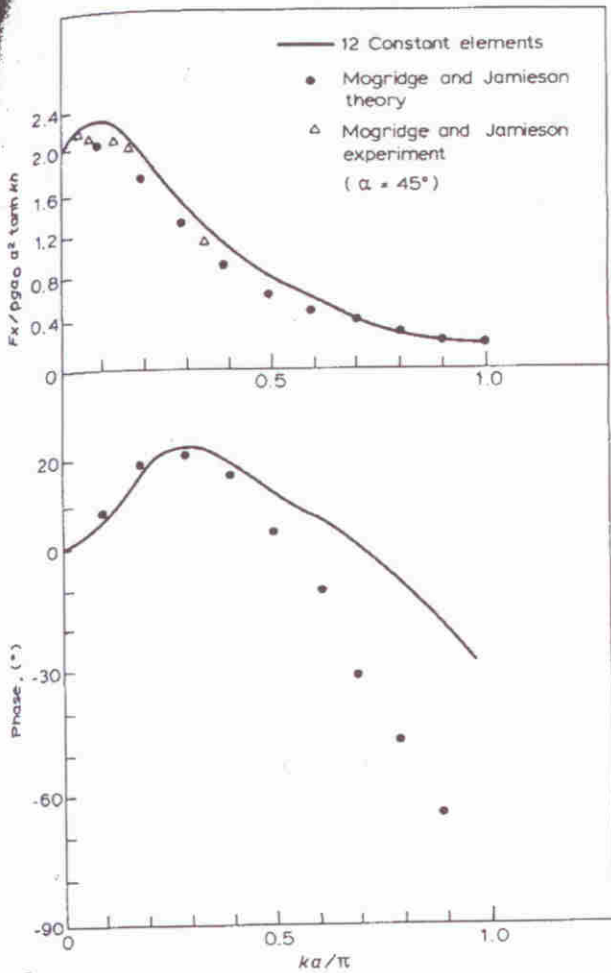


Figure 14 Magnitude and phase of horizontal force on a square caisson

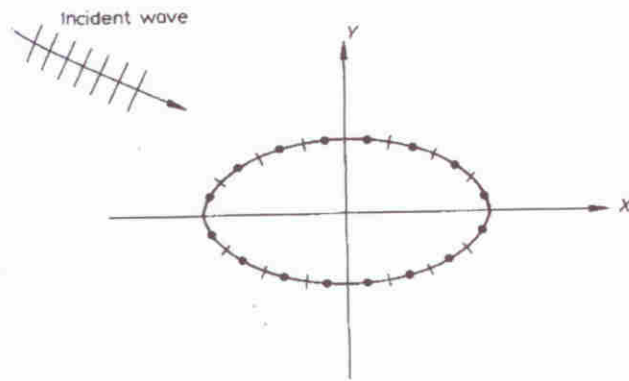


Figure 15 Elliptical section ($X^2/a^2 + Y^2/b^2 = 1$). $a = 10$; $b/a = 0.15$; $h/a = 1$

studies are usually carried out using the equivalent cylinder approach.

Elliptical cylinder

The third example is a cylinder of elliptical cross section (Figure 15). This case gives much more complex results than the previous two.

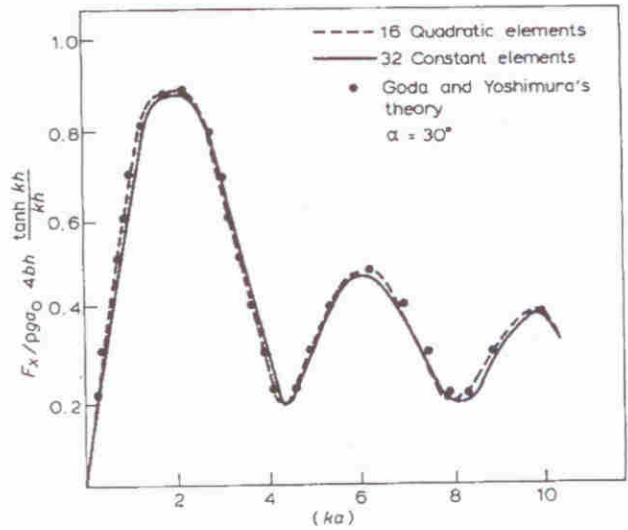


Figure 16 F_x forces on elliptical cylinder

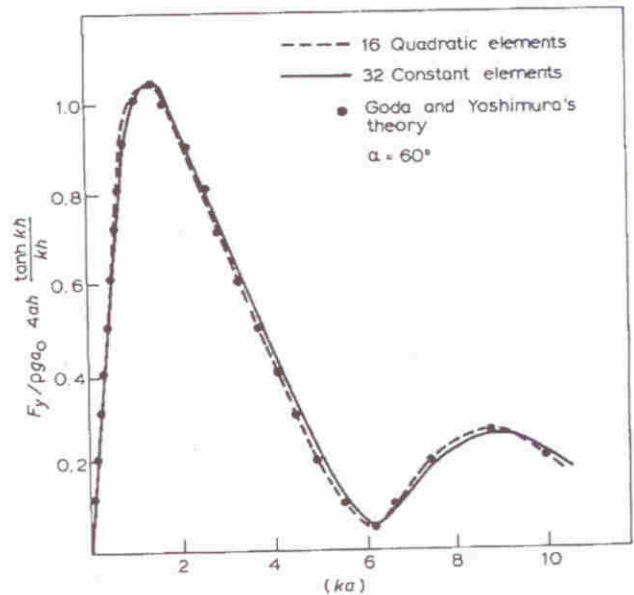
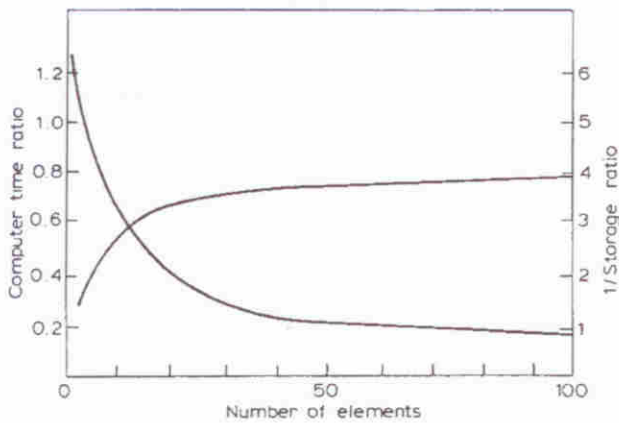


Figure 17 F_y force on elliptical cylinder

An analytical solution has been presented by Goda and Yoshimi.² They solved the Helmholtz equation by using separation of variables and obtained a close form solution. The boundary element solution was obtained using 32 constant elements with smaller elements near the major axis of the ellipse (Figure 15) to take into consideration the more rapid change of the slope at that position. The horizontal forces were obtained for two α angles for the incident wave, i.e. $\alpha = 30^\circ$ and $\alpha = 60^\circ$. Results are plotted in Figures 16 and 17 and good agreement was found with the results presented in reference 2.

It was then decided to apply symmetry in order to obtain a smaller system of equations and try to find out if symmetry would introduce any numerical approximations. One quarter of the structure (Figure 5) was discretized using eight constant elements. Results were found to be exactly the same as those using 32 elements. Then the



computer storage and time used for the case of considering or not symmetry were obtained to complete the analysis. The results presented as a ratio are presented in Figure 18. Results were also obtained using 16 quadratic elements to represent the whole cylinder. These results validate the constant element solution and the proposed treatment of symmetry.

Note that when the number of elements increases the symmetry solution requires only 25% of the total storage and 20% of the computer time required for the case of solving the full problem. This shows the advantages of implementing symmetry conditions in boundary element programs.

Conclusions

The present paper has presented an application of the boundary element method for computing wave forces on offshore structures. The paper compares solutions obtained using constant, linear and quadratic elements and critically discusses their accuracy and convergence. It also shows how symmetry conditions can be introduced and their importance in order to reduce computer time and storage in many cases. The examples studied and their comparison with other solutions validate the use of boundary elements to study wave diffraction and, in particular, points out the simplicity of this approach by comparison with solutions such as finite differences and finite elements.

References

- 1 MacCamy, R. C. and Fuchs, R. A. 'Wave force on a pile: a diffraction theory', *Tech. Memo 69*. US Army Corps of Engineers Beach Erosion Board, Washington DC, 1954
- 2 Goda, Y. and Yoshimura, T. 'Wave force on a vessel tied at offshore dolphins'. Chap. 96, *Proc. 13th Coastal Eng. Conf.*, Vol. III, pp. 1723-1742, 1972
- 3 Ijima, T., Chou, C.-R. and Yumura, Y. 'Wave scattering by permeable and impermeable breakwater of arbitrary shape'. Chap. 11, *Proc. 14th Coastal Eng. Conf.*, Vol. III, pp. 1886-1905, 1974
- 4 Isaacson, M. de St. Q. 'Vertical cylinder of arbitrary section in wave', *J. Waterway, Port, Coastal and Ocean Div.*, ASCE, 1978, 104, 309
- 5 Harms, V. W. 'Diffraction of water waves by isolated structures', *J. Waterway, Port, Coastal and Ocean Div.*, ASCE, 1979, 105, 131
- 6 Hwang, L. S. and Tuck, E. O. 'On the oscillations of harbours of arbitrary shape', *J. Fluid Mech.*, 1970, 42, 447
- 7 Rahman, M. 'Numerical response of an arbitrary shaped harbour', *Appl. Math. Modelling*, 1981, 5, 109
- 8 Brebbia, C. A. 'The boundary element methods for engineers', Pentech Press, London, 1978
- 9 Brebbia, C. A. and Walker, S. 'Boundary element techniques in engineering', Newnes-Butterworths, London, 1980
- 10 Brebbia, C. A. (ed.). 'Progress in boundary element methods', Vol. 1, Pentech Press, London; Wiley, NY, 1981
- 11 Berkhoff, J. C. W. 'Linear wave propagation problems and the finite element method', Chap. 13 'Finite elements in fluids', Vol. 1 (Gallagher, R. H., et al. (eds.), 1975
- 12 Modridge, G. R. and Jamieson, W. W. 'Wave forces on square caissons', Chap. 133, *Proc. 15th Coastal Eng. Conf.*, ASCE, pp. 2271-2289, 1976

Appendix

The Hankel function of the first kind of zero order is defined as:

$$H'_0(x) = J_0(x) + iY_0(x) \quad (A1)$$

Its derivative is:

$$\frac{d}{dx} [H'_0(x)] = -J_1(x) - iY_1(x) \quad (A2)$$

For large X :

$$H'_0(X) = \sqrt{\frac{2}{\pi X}} \exp[i(x - \pi/4)] \quad (A3)$$

For small x and up to second order:

$$J_0(x) = 1 - \frac{x^2}{4} \quad (A4)$$

$$Y_0(x) = \frac{2}{\pi} \left\{ \left(\gamma + \ln \frac{x}{2} \right) \left(1 - \frac{x^2}{4} \right) + \frac{x^2}{4} \right\}$$

$$J'_0(x) = -\frac{x}{2} \quad (A5)$$

$$Y'_0(x) = \frac{2}{\pi} \left\{ \frac{x}{2} \left(0.5 - \gamma - \ln \frac{x}{2} \right) + \frac{1}{x} \right\}$$

$$\gamma = 0.577216 \dots$$